Effects of polarization on the transmission and localization of classical waves in weakly scattering metamaterials

Ara A. Asatryan,[1] Lindsay C. Botten,[1] Michael A. Byrne,[1] Valentin D. Freilikher,[2] Sergey A. Gredeskul,[3,4] Ilya V. Shadrivov,[4] Ross C. McPhedran,[5] and Yuri S. Kivshar[4,6]

[1]*Department of Mathematical Sciences, Centre for Ultrahigh-bandwidth Devices for Optical Systems (CUDOS), University of Technology, Sydney, New South Wales 2007, Australia*

[2]*Department of Physics, Bar-Ilan University, Raman-Gan 52900, Israel*

[3]*Department of Physics, Ben Gurion University of the Negev, Beer Sheva 84105, Israel*

[4]*Nonlinear Physics Center and CUDOS, Research School of Physics and Engineering, Australian National University, Canberra, Australian Capital Territory 0200, Australia*

[5]*School of Physics and CUDOS, University of Sydney, Sydney, New South Wales 2006, Australia*

[6]*St. Petersburg State University of Information Technologies, Mechanics and Optics, 197101 St. Petersburg, Russia*

(Received 13 August 2010; revised manuscript received 2 November 2010; published 29 November 2010)

We summarize the results of our comprehensive analytical and numerical studies of the effects of polarization on the Anderson localization of classical waves in one-dimensional random stacks. We consider homogeneous stacks composed entirely of normal materials or metamaterials, and also mixed stacks composed of alternating layers of a normal material and a metamaterial. We extend the theoretical study developed earlier for the case of normal incidence [A. A. Asatryan *et al.*, Phys. Rev. B **81**, 075124 (2010)] to the case of off-axis incidence. For the general case where both the refractive indices and layer thicknesses are random, we obtain the long-wave and short-wave asymptotics of the localization length over a wide range of incidence angles (including the Brewster "anomaly" angle). At the Brewster angle, we show that the long-wave localization length is proportional to the square of the wavelength, as for the case of normal incidence, but with a proportionality coefficient substantially larger than that for normal incidence. In mixed stacks with only refractive-index disorder, we demonstrate that *p*-polarized waves are strongly localized, while for *s* polarization the localization is substantially suppressed, as in the case of normal incidence. In the case of only thickness disorder, we study also the transition from localization to delocalization at the Brewster angle.

DOI: 10.1103/PhysRevB.82.205124 PACS number(s): 42.25.Dd, 42.25.Fx

I. INTRODUCTION

Anderson localization is one of the most fundamental and fascinating phenomena in the physics of disordered systems. Predicted in the seminal paper of Anderson[1] for spin excitations and extended to the case of electrons and other one-particle excitations in solids (see, for example, Ref. 2) and also applied to classical waves,[3] this very general phenomenon has become a paradigm of modern physics.[4] Despite considerable efforts, the theoretical framework of Anderson localization in higher dimensions ($D>1$) is far from complete,[5] especially in the case of classical waves where the effects of absorption,[6] gain,[7,8] and polarization[9–11] are significant.

In contrast, the one-dimensional case ($D=1$) has been studied extensively for both quantum mechanical and classical waves (see, e.g., Refs. 2 and 12). In the systems with short-range correlated disorder, it is known that all states are localized.[13,14] One of the main manifestations of localization is the exponential decay of the amplitude of a wave propagating through an infinite disordered sample. This decay is the result of the interference of multiply scattered waves, and its spatial rate is called the Lyapunov exponent, γ, whose inverse value γ^{-1} is a characteristic length describing localization in an infinite sample. By itself, however, the reciprocal of the Lyapunov exponent does not provide comprehensive information about the transport properties of disordered media for all cases (see Ref. 24 for details). Moreover, it is unlikely that this quantity can be measured directly, at least in the optical regime.

A further manifestation of localization is the exponential decay of the transmission coefficient of a long, finite sample. The characteristic length of this decay is the transmission length l_T, also denoted by l_N in the case of a sample of N layers. In the localized regime, where this length is much smaller than the sample size, in general, the transmission length coincides with the localization length l, and also with the inverse Lyapunov exponent γ^{-1}.

The Anderson localization of classical waves in one-dimensional disordered systems has been studied in detail[8,9,15–17] and it has been shown that in the long-wave region where the interference is weak, the localization length demonstrates a universal behavior, growing in proportion to the square of the wavelength, i.e., $l \propto \lambda^2$.

In recent years, we have witnessed the rapid emergence of a new field of research in metamaterials—artificial materials which exhibit a negative refractive index.[19–22] In such materials, the wave vector **k**, the electric field vector **E**, and the magnetic field vector **H** form a left-handed coordinate system, in contrast to the right-handed system that is applicable to normal or regular materials; for this reason, metamaterials are sometimes referred to as left-handed materials. In metamaterials, the directions of the phase velocity and the energy flow are opposite. This feature can strongly affect Anderson localization in metamaterials. Indeed, in stratified media formed of alternating layers of normal materials and

 ©2010 The American Physical Society

metamaterials, the phase accumulated during propagation through a right-handed layer diminishes in its propagation in a left-handed layer[23] and, as a consequence, interference will be weakened and localization suppressed.

Already, one of the first study[23] of Anderson localization in the presence of metamaterials has revealed the striking behavior that in the particular case of an alternating stack of right- and left-handed layers of the same thickness and randomly varying refractive indices, the localization is strongly suppressed. Its functional form in the long-wave region changes from the standard behavior of $l \propto \lambda^2$ to $l \propto \lambda^6$ and, subsequently, it was shown[24] that in such stacks the localization length differs from the inverse of the Lyapunov exponent—the first such example of this surprising behavior.

While the disorder is one dimensional, the random stacks are actually three-dimensional objects and so the vector nature of the propagating field and, in particular, its polarization can strongly influence localization, leading to its suppression or even complete delocalization. For stacks comprising only normal layers, the effects of polarization have been extensively studied. The problem has been studied using an approach based on stochastic differential equations[9] with excellent agreement obtained at short wavelengths (for normal incidence), and also in the long-wavelength limit, between the theoretically predicted localization length and that obtained by direct simulation. The delocalization associated with the Brewster angle anomaly has been studied in the long-wave limit using an effective medium approach,[10] and at short wavelengths in the framework of a random-phase approximation.[11] Numerical simulations for the off-axis case are given in Ref. 25 while, in Ref. 26, the polarization properties of localization have been considered experimentally.

Although the approaches described in Refs. 8–11, 25, and 26 give rich information about the effects of polarization on the properties of localization in normal materials, a general expression for the localization length, applicable for broad range of input parameters (including at the Brewster anomaly angle) is still missing. Furthermore, there are no results available for the effects of polarization on localization in the presence of metamaterials.

In this paper, we extend our earlier study[24] to the case of off-axis incidence and provide a comprehensive analytical and numerical treatment of the effects of polarization on the localization length l. We consider both homogeneous stacks, formed by only normal material layers or by only metamaterial layers and also mixed stacks formed by an alternating sequence of right- and left-handed layers with random thicknesses and refractive indices. We derive explicit asymptotic expressions for the localization length at the short- and long-wavelength limits that are applicable for the Brewster angle and demonstrate their excellent agreement with direct simulation.

The paper is organized as follows. In Sec. II, we describe the model and outline the theoretical treatment. The derivation of the asymptotic forms for the localization length at short and long wavelengths is presented in Sec. III. In Sec. IV, we present the results of numerical simulations for the localization length for s and p polarizations in both homogeneous and mixed stacks. Here, we adopt the conventional definition for polarization with s and p polarization referring, respectively, to the cases in which the electric and magnetic fields are perpendicular to the plane of incidence. Finally, in Sec. V, the dependence of the localization length on the angle of incidence, at a fixed wavelength, is considered.

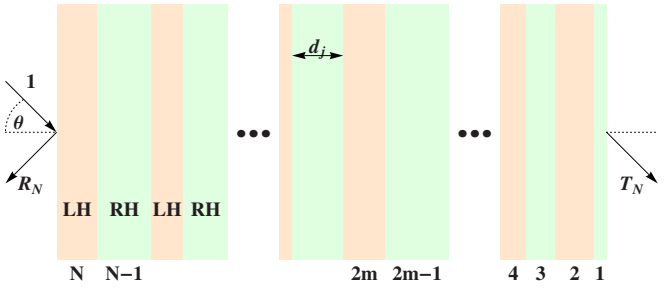

FIG. 1. (Color online) The geometry of the structure.

II. THEORETICAL STUDIES

A. Model

We consider the transmission and localization properties of a one-dimensional, multilayered, disordered stack which consists of N layers composed of either right-handed or normal (r) materials, left-handed (l) metamaterials, or mixed stacks comprising alternating layers (r and l) of each (see Fig. 1).

All layers are statistically independent and, in the most general case, the thickness of each layer, and its dielectric and magnetic permittivities, are random quantities with given probability densities. All lengths in the problem are measured in the unit of the mean layer thickness and, therefore, are dimensionless quantities.

The main subject of our interest is the transmission length[2,4]

$$l_N = -\frac{N}{\langle \ln|T_N| \rangle}, \tag{1}$$

where T_N is the transmission coefficient of the N layer stack for a plane wave with a given incidence angle (relative to the surface normal of the stack). Angular brackets are used to denote averaging over realizations of all random parameters. In the limit of a stack of infinite length, i.e., $N \to \infty$, the transmission length coincides with the localization length, i.e.,

$$l = \lim_{N \to \infty} l_N. \tag{2}$$

The calculation of the transmission length Eq. (1) requires the transmission coefficient T_N of the N-layer stack for a wave of a given polarization and a given incidence angle. Such a calculation can be based on the transfer-matrix method,[15] the interface iteration method,[8] and the layer iteration method.[23] We choose the last of these and build on the treatment that was used successfully in our previous study[24] for the case of normal incidence.

The method is based on the *exact* iteration of the recurrence relations

$$T_n = \frac{T_{n-1}t_n}{1 - R_{n-1}r_n}, \tag{3}$$

$$R_n = r_n + \frac{R_{n-1}t_n^2}{1 - R_{n-1}r_n} \tag{4}$$

for the total transmission T_n and total reflection R_n coefficients of a n-layer stack, $n=1,\ldots,N$, in which both the input and output media are free space and with initial conditions set to $T_0=1$ and $R_0=0$. Here t_n and r_n are the transmission and reflection coefficients of the nth layer with layers being enumerated from $n=1$ at the rear of the stack through to $n=N$ at the front.

Such an approach is quite general and is applicable to an arbitrary choice of polarization (s) or (p), the angle of incidence θ, the type of layer (r or l), the wavelength λ, and the amount of absorption or gain. All these input data are incorporated into the transmission and reflection characteristics t_n and r_n of a single layer.

The recurrence relations in Eqs. (3) and (4) together with the definitions in Eqs. (1) and (2) enable the numerical calculation of the transmission length l_N in the most general case. If the calculated transmission length l_N is much smaller than the stack length N and is independent of N, then l_N may be identified as the localization length, i.e., $l_N=l$.

In the work reported in this paper, we deal with a specific model in which the dimensionless thicknesses d of each layer are independent, identically distributed, random variables, $d=1+\delta_d$, where δ_d is uniformly distributed in the range $[-Q_d,Q_d]$ with $0\leq Q_d<1$. The dielectric and magnetic permittivities of the layers are represented in the form

$$\varepsilon = \pm(1+\delta_\nu)^2, \quad \mu = \pm 1, \tag{5}$$

where the upper and lower signs, respectively, correspond to a normal material or a metamaterial. The random part δ_ν of the refractive index,

$$\nu = \pm(1+\delta_\nu), \tag{6}$$

is uniformly distributed in the range $[-Q_\nu,Q_\nu]$, $0\leq Q_\nu<1$. Accordingly, the model takes into account both refractive-index disorder and layer thickness disorder.

B. Theoretical analysis

Our theoretical treatment is based on a weak scattering approximation (WSA) in which the magnitude of the reflection coefficient of each layer $|r_n|\ll 1$ is the primary small parameter in the theory. To understand when this condition is valid and may be used, we next consider explicit expressions for the reflection r and transmission t coefficients of any single layer

$$r = \frac{\rho(1-e^{2i\beta})}{1-\rho^2 e^{2i\beta}}, \quad t = \frac{(1-\rho^2)e^{i\beta}}{1-\rho^2 e^{2i\beta}}, \tag{7}$$

where ρ is Fresnel interface reflection coefficient given by

$$\rho = \frac{\cos\theta - \mathcal{Z}\cos\theta_\nu}{\cos\theta + \mathcal{Z}\cos\theta_\nu}, \quad \mathcal{Z} = \begin{cases} Z^{-1} & s \text{ polarization} \\ Z & p \text{ polarization.} \end{cases} \tag{8}$$

In these equations,

$$\beta = kd\nu\cos\theta_\nu, \quad \cos\theta_\nu = \sqrt{1-\frac{\sin^2\theta}{\nu^2}}, \quad k = 2\pi/\lambda, \tag{9}$$

λ is the dimensionless free space wavelength and

$$Z = \sqrt{\frac{\mu}{\varepsilon}} = \frac{1}{1+\delta_\nu} > 0 \tag{10}$$

is the layer impedance relative to the background (free space).

There are two cases in which the magnitude of the single-layer reflection coefficient is small, i.e., $|r|\ll 1$. The first is characterized by weak refractive-index disorder $Q_\nu \ll 1$ and corresponds to the incidence angle θ being smaller than its critical value

$$\theta_c = \sin^{-1}(1-Q_\nu). \tag{11}$$

In this case it is the small magnitude of the Fresnel reflection coefficient $|\rho|\ll 1$ which leads to a small, single-layer reflection coefficient ($|r|\ll 1$) at all wavelengths. The second case corresponds to the long-wavelength limit ($\lambda \gg 1$) in which the single-layer reflection coefficient is small ($|r|\ll 1$) for an arbitrary incidence angle θ due to the asymptotically small value of the multiplier $|1-e^{2i\beta}|\propto\beta\ll 1$ which appears in the expression for r in Eq. (7).

Within the WSA approximation, we commence the derivation of general forms with the linearized recurrence relations in Eq. (4)

$$\ln T_n = \ln T_{1,n-1} + \ln t_n + R_{n-1}r_n,$$

$$R_n = r_n + R_{n-1}t_n^2, \tag{12}$$

and solve them to yield

$$\ln T_N = \sum_{j=1}^{N} \ln t_j + \sum_{m=2}^{N}\sum_{j=m}^{N} r_{j-m+1}r_j \prod_{p=j-m+2}^{j-1} t_p^2, \tag{13}$$

from which we may compute ensemble averages. In what follows, we summarize the key theoretical results[24] applicable to mixed and homogeneous stacks.

1. Mixed stacks

A mixed stack, which hereafter is abbreviated by M-stack, is composed of alternating layers of right-handed (r) and left-handed (l) materials (see Fig. 1). Within the model, there are simple relations that may be derived[24] between the averaged values of an analytic function g of the transmission and reflection characteristics of single layers of left- and right-handed materials,

$$\langle g(t_r)\rangle = \langle g(t_l)\rangle^*, \quad \langle g(r_r)\rangle = \langle g(r_l)\rangle^*. \tag{14}$$

As a consequence, the transmission length of a M-stack depends only on the properties of a single right-handed layer and is expressible in terms of only three averaged quantities: $\langle r\rangle^2$, $\langle \ln t\rangle$, and $\langle t^2\rangle$, in which the subscript r (referring to a right-handed layer) has been omitted

$$\frac{1}{l_N} = \frac{1}{l} + \left(\frac{1}{b} - \frac{1}{l}\right) f\left(\frac{N}{\bar{l}_m}\right). \tag{15}$$

Here,

$$\frac{1}{l} = -\,\mathrm{Re}\langle \ln t\rangle - \frac{|\langle r\rangle^2| + \mathrm{Re}(\langle r\rangle^2\langle t^2\rangle^*)}{1 - |\langle t^2\rangle|^2} \tag{16}$$

is the inverse localization length,

$$\frac{1}{b} = \frac{1}{l} - \frac{2/\bar{l}_m}{1 - \exp(-2/\bar{l}_m)} \times \left(\frac{|\langle r\rangle^2| + \mathrm{Re}(\langle r\rangle^2\langle t^2\rangle^*)}{1 - |\langle t^2\rangle|^2} - \frac{|\langle r\rangle^2|}{2}\right) \tag{17}$$

is the inverse ballistic length, and

$$f(z) = \frac{1 - \exp(-z)}{z}. \tag{18}$$

To characterize the transition from localization to ballistic propagation, we introduce the *crossover length* for a M-stack,[24]

$$\bar{l}_m = -\frac{1}{\ln|\langle t^2\rangle|}, \tag{19}$$

and two characteristic wavelengths λ_1 and λ_2 defined by

$$N = l[\lambda_1(N)], \quad N = \bar{l}[\lambda_2(N)]. \tag{20}$$

For long wavelengths, that part of the spectrum for which $\lambda \ll \lambda_1(N)$ corresponds to the localization regime, for which $l_N = l$. In turn, the wavelength range $\lambda \gg \lambda_2(N)$ corresponds to ballistic propagation and $l_N = b$. The region $\lambda_1 < \lambda < \lambda_2$ is the transition region from localization to ballistic propagation. In what follows, we characterize these regions with long-wavelength asymptotes for the localization length l and the crossover length $\bar{l}$.

2. Homogeneous stacks

The homogeneous stack (abbreviated from here as a H-stack) is composed of layers of the same type of material (either r or l). By virtue of the symmetry relations in Eq. (14), the results for statistically equivalent stacks of either normal materials or metamaterials are identical.

The transmission length of a H-stack is then

$$\frac{1}{l_N} = \frac{1}{l} + \frac{1}{N}\mathrm{Re}\left[\langle r\rangle^2 \frac{1 - \langle t^2\rangle^N}{(1 - \langle t^2\rangle)^2}\right] \tag{21}$$

while the inverse localization length is given by

$$\frac{1}{l} = -\,\mathrm{Re}\langle \ln t\rangle - \mathrm{Re}\frac{\langle r\rangle^2}{1 - \langle t^2\rangle}. \tag{22}$$

It follows from Eq. (21) that the crossover length $\bar{l}_h$ of the H-stack is

$$\bar{l}_h = -\frac{1}{|\ln\langle t^2\rangle|}, \tag{23}$$

characterizing the transition from the near ballistic regime to the far ballistic regime of propagation.

III. ASYMPTOTIC BEHAVIOR OF THE TRANSMISSION AND LOCALIZATION LENGTHS

The results in Eqs. (15)–(17), (21), and (22) for the transmission, localization and ballistic lengths of homogeneous and mixed stacks are quite general. In this section we apply them to the specific model described in Sec. II A. We emphasize that within the model both two types of disorder are present and are taken into account in all intermediate calculations. However, in all final results we keep only the leading terms. The higher order corrections with respect to the relative perturbations $Q_{\nu,d}$ of the refractive index and thickness distributions are generally omitted.

A. Short-wave asymptotics of the transmission length

When the incidence angle θ is smaller than the critical angle θ_c [Eq. (11)], the short-wavelength asymptotics of the localization length can be easily obtained from Eqs. (16) and (22). At short wavelengths, the phase of the field is a strongly fluctuating, random quantity so that $\langle t^2\rangle \approx 0$, $\langle r\rangle \approx \langle \rho\rangle$, and $\langle \ln|t|\rangle \approx \langle \ln(1-\rho^2)\rangle$. As a consequence, the localization length for both mixed and homogeneous stacks takes the form

$$\frac{1}{l} = -\langle \ln(1 - \rho^2)\rangle - \langle \rho\rangle^2. \tag{24}$$

For s polarization, the logarithmic term in Eq. (24) always dominates and so

$$\frac{1}{l} \approx \frac{Q_\nu^2}{12\cos^4\theta} \tag{25}$$

while the second term in Eq. (24) provides a higher order correction of order $O(Q_\nu^4)$. For p polarization, however, the corresponding correction cannot be omitted since the first term vanishes at the Brewster angle $\theta = \pi/4$. Thus, for p polarization,

$$\frac{1}{l} \approx \frac{Q_\nu^2 \cos^2(2\theta)}{12\cos^4\theta} + \frac{Q_\nu^4}{120\cos^8\theta} \times \left(\frac{569}{96} - 8\cos 2\theta + \frac{43}{8}\cos 4\theta + \cos 6\theta + \frac{11}{96}\cos 8\theta\right). \tag{26}$$

Accordingly, at the Brewster angle, the localization length is given by

$$l = \frac{45}{4Q_\nu^4}. \tag{27}$$

Note that in the case of normal incidence, the results in Eqs. (25) and (26) coincide with those presented in Refs. 8, 9, 15, and 16.

If the incidence angle θ exceeds the critical angle θ_c [Eq. (11)], then total internal reflection occurs (i.e., the magnitude of the Fresnel reflection coefficient becomes unity) and so the WSA fails in the short-wave region. If the incident angle is sufficiently far above the critical value θ_c, then the exponent $2i\beta$ in Eq. (7) is real and negative and thus the magnitude of the single-layer transmission coefficient is exponen-

tially small. As a result, we obtain the following expression for the transmission length:

$$\frac{1}{l_N} = \mathrm{Im}\langle\beta\rangle = k\ \mathrm{Im}\langle d\sqrt{\sin^2\theta - \nu^2}\rangle, \quad \text{for} \quad \sin\theta > 1 - Q_\nu. \tag{28}$$

The right-hand side of this equation is independent of the stack length N and so it formally coincides with the inverse localization length l. However, its origin is related to attenuation by tunneling, rather than to Anderson localization. In the attenuation regime, the transmission length does not distinguish the left- and right-handed layers since it depends on the square of the refractive index ν and so is the same for equivalent l or r layer. Moreover, it does not distinguish the polarization of the light.

The average of Eq. (28) can be calculated in closed form for the uniform distribution of the refractive index and we obtain the short-wave asymptotic of the transmission length in the attenuation regime from the expression

$$\frac{1}{l_N} = \frac{k}{4Q_\nu}\left[\left(\frac{\pi}{2} - \sin^{-1}\frac{1-Q_\nu}{\sin\theta}\right)\sin^2\theta - (1 - Q_\nu)\sqrt{\sin^2\theta - (1-Q_\nu)^2}\right], \tag{29}$$

and see that it is proportional to the wavelength. We see also that it holds for both polarizations, and also for both H- and M-stacks.

The main contribution to this length in the short-wave region coincides with that of the first terms in Eqs. (16) and (22) for the localization lengths of H- and M-stacks. These terms in Eqs. (16) and (22) dominate in the short-wave region, as we will demonstrate below, and thus these terms give the correct values for the transmission length in the attenuation regime (for both short-wave and long-wave regions) despite the applicability of the WSA being violated.

B. Long-wave asymptotics for homogeneous stacks

1. Homogeneous stacks: s polarization

For long wavelengths, the transmission length can be deduced from the general result in Eq. (22). In this limit, the mean values of $\langle \ln t\rangle$, $\langle t^2\rangle$, and $\langle r\rangle$ that enter Eq. (22) for s polarization take the form

$$\langle \ln t\rangle = ik\cos\theta + \frac{ikQ_\nu^2}{6\cos\theta} - \frac{k^2Q_\nu^2}{6\cos^2\theta}\left(1 + \frac{Q_d^2}{3}\right) - \frac{k^2Q_\nu^4}{40\cos^2\theta}\left(1 + \frac{Q_d^2}{3}\right), \tag{30}$$

$$\langle r\rangle = \frac{ikQ_\nu^2}{6\cos\theta} - \frac{k^2Q_\nu^2}{6\cos^2\theta}\left(2 + \cos^2\theta + \frac{3Q_\nu^2}{10}\right)\left(1 + \frac{Q_d^2}{3}\right) - \frac{ik^3Q_\nu^2}{9\cos\theta}(4 + \cos^2\theta)(1 + Q_d^2) - \frac{ik^3Q_\nu^4}{2\cos^3\theta}\left(\frac{2}{3} + \frac{\cos 2\theta}{15} + \frac{Q_\nu^2}{28}\right)(1 + Q_d^2), \tag{31}$$

$$\langle t^2\rangle = 1 + 2ik\cos\theta + \frac{ikQ_\nu^2}{3\cos\theta} - 2k^2\cos^2\theta - \frac{2k^2Q_d^2}{3}\cos^2\theta - \frac{k^2Q_\nu^2}{3\cos^2\theta}(3 + 2\cos^2\theta) \times\left(1 + \frac{Q_d^2}{3}\right) - \frac{3k^2Q_\nu^4}{20\cos^2\theta}\left(1 + \frac{Q_d^2}{3}\right). \tag{32}$$

Applying the results of Eqs. (30)–(32) in the expression for the transmission length Eq. (21), we obtain

$$\frac{1}{l_N} = \frac{k^2Q_\nu^2}{6\cos^2\theta}\left(1 + \frac{Q_\nu^2}{15} - \frac{Q_\nu^2}{3\cos^2\theta}\right)\left(1 + \frac{Q_d^2}{3}\right) + \frac{Q_\nu^4}{72\cos^4\theta}\left(\frac{\sin^2(kN\cos\theta)}{N}\right), \tag{33}$$

which is correct to the order of Q_ν^4. This expression can be further simplified given that $Q_\nu \ll 1$ and $Q_d \ll 1$. In this approximation, the transmission length takes form

$$\frac{1}{l_N} = \frac{k^2Q_\nu^2}{6\cos^2\theta}\left[1 + \frac{NQ_\nu^2}{12}\left(\frac{\sin(kN\cos\theta)}{kN\cos\theta}\right)^2\right], \tag{34}$$

from which it follows that the localization length is given by

$$l = \frac{3\lambda^2\cos^2\theta}{2\pi^2Q_\nu^2}, \quad l \le N. \tag{35}$$

From this, it is seen that the localization length of a homogeneous stack in the long-wavelength limit does not depend on the thickness disorder for s polarization. We verified this through exact numerical calculations (see Fig. 2).

Equation (35) reproduces the result first derived in Ref. 9 and, for normal incidence, coincides with the localization length derived more recently in Refs. 18 and 24. For wavelengths such that $l \ge N \ge \lambda/\cos\theta$, there is a near ballistic regime where the ballistic length b is the same as the localization length

$$b = \frac{3\lambda^2\cos^2\theta}{2\pi^2Q_\nu^2}, \quad l \ge N \ge \frac{\lambda}{\cos\theta}. \tag{36}$$

The crossover length in the far ballistic region Eq. (23) is

$$\bar{l}_h = \frac{\lambda}{4\pi\cos\theta} \tag{37}$$

while the ballistic length b_f in this region is

$$b_f = \frac{3\lambda^2\cos^2\theta}{2\pi^2Q_\nu^2}\left[1 + \frac{NQ_\nu^2}{12}\right]^{-1}. \tag{38}$$

From Eqs. (20), (35), and (37), it follows that

$$\lambda_1 = \frac{\pi Q_\nu}{\cos\theta}\sqrt{\frac{2N}{3}}, \tag{39}$$

$$\lambda_2 = 4\pi N \cos\theta \tag{40}$$

for all reasonable values of the input parameters such that $\lambda_1 < \lambda_2$. For $\lambda < \lambda_1$, waves are localized with the localization length given by Eq. (35). The wavelength range $\lambda_1 < \lambda < \lambda_2$ corresponds to the near ballistic regime in which the ballistic length b is given by Eq. (36). The longer wavelengths, $\lambda \geq \lambda_2$, correspond to the far ballistic regime in which the ballistic length b_f is given by Eq. (38).

2. Homogeneous stacks: p polarization

In the case of p-polarized waves, the mean values of $\langle \ln t\rangle$, $\langle t^2\rangle$, and $\langle r\rangle^2$, at longer wavelengths, take the form

$$\begin{aligned}\langle \ln t\rangle = {} & ik\cos\theta + \frac{ikQ_\nu^2\cos 3\theta}{6\cos^2\theta} - \frac{ikQ_\nu^4\sin^2\theta}{2\cos\theta}(1+Q_\nu^2) \\ & - \frac{k^2Q_\nu^2\cos^2 2\theta}{6\cos^2\theta}\left(1+\frac{Q_d^2}{3}\right) \\ & - \frac{k^2Q_\nu^4}{40\cos^2\theta}(2-3\cos 2\theta)^2\left(1+\frac{Q_d^2}{3}\right) \\ & - \frac{k^2Q_\nu^6\tan^2\theta}{4}(2-3\cos\theta),\end{aligned} \tag{41}$$

$$\begin{aligned}\langle r\rangle = {} & -\frac{ikQ_\nu^2(2-\cos 2\theta)}{6\cos\theta} - \frac{ikQ_\nu^4\sin^2\theta}{2\cos\theta}(1+Q_\nu^2) \\ & + \frac{k^2Q_\nu^2}{24\cos^2\theta}(3+10\cos 2\theta-\cos 4\theta)\left(1+\frac{Q_d^2}{3}\right) \\ & - \frac{k^2Q_\nu^4}{80\cos^2\theta}(31-52\cos 2\theta+17\cos 4\theta)\left(1+\frac{Q_d^2}{3}\right) \\ & - \frac{k^2Q_\nu^6\tan^2\theta}{2}(2-3\cos 2\theta) + ak^3,\end{aligned} \tag{42}$$

$$\begin{aligned}\langle t^2\rangle = {} & 1 + 2ik\cos\theta - 2k^2\cos^2\theta + \frac{ikQ_\nu^2\cos 3\theta}{6\cos^2\theta} \\ & - \frac{k^2Q_\nu^2}{3\cos^2\theta}(2\cos^2\theta + 3\cos^2 2\theta) - \frac{2k^2Q_d^2}{3}\cos^2\theta,\end{aligned} \tag{43}$$

where the expression for the coefficient of the cubic term a in Eq. (42) is given in the Appendix. The transmission length l_N, given by Eq. (21), can then be expressed in the asymptotic expansion form as

$$\begin{aligned}\frac{1}{l_N} = {} & \frac{k^2Q_\nu^2\cos^2 2\theta}{6\cos^2\theta}\left(1+\frac{Q_d^2}{3}\right) + \frac{k^2Q_\nu^4}{24\cos^4\theta}h_1(\theta)\left(1+\frac{Q_d^2}{3}\right) \\ & + \frac{k^2Q_\nu^6}{17280\cos^6\theta}h_2(\theta) \\ & + \frac{Q_\nu^4}{18N\cos^4\theta}\left(\frac{3}{2}-\cos^2\theta\right)^2\sin^2(kN\cos\theta),\end{aligned} \tag{44}$$

where

$$h_1(\theta) = 1 - \frac{19}{6}\cos 2\theta + \frac{7}{15}\cos 4\theta + \frac{19}{30}\cos 6\theta, \tag{45}$$

$$\begin{aligned}h_2(\theta) = {} & 1415 - 1664\cos 2\theta - 188\cos 4\theta + 512\cos 6\theta \\ & + 141\cos 8\theta.\end{aligned} \tag{46}$$

This expression can be further simplified given $Q_\nu \ll 1$ and $Q_d \ll 1$. We obtain the final form of the transmission length correct to the order of $O(Q_\nu^4)$

$$\begin{aligned}\frac{1}{l_N} = {} & \frac{k^2Q_\nu^2\cos^2 2\theta}{6\cos^2\theta}\left(1+\frac{Q_d^2}{3}\right) + \frac{k^2Q_\nu^4}{24\cos^4\theta}h_1(\theta) \\ & + \frac{Q_\nu^4}{18N\cos^4\theta}\left(\frac{3}{2}-\cos^2\theta\right)^2\sin^2(kN\cos\theta)\end{aligned} \tag{47}$$

with the localization length being given by

$$\frac{1}{l} = \frac{k^2Q_\nu^2\cos^2 2\theta}{6\cos^2\theta} + \frac{k^2Q_\nu^2Q_d^2\cos^2 2\theta}{18\cos^2\theta} + \frac{k^2Q_\nu^4}{24\cos^4\theta}h_1(\theta), \tag{48}$$

where $h_1(\theta)$ is given by Eq. (45). We have verified numerically the asymptotic formula (48) in Sec. V A and found that it is in excellent agreement with the exact numerical calculations for angles of incidence of up to 80°.

Equation (48) generalizes the corresponding expression for the localization length obtained in Ref. 9 and is applicable to incidence at the Brewster anomaly angle of $\theta = \pi/4$. At this angle, the first two terms in Eq. (48) vanish, leading to

$$l = \frac{45\lambda^2}{16\pi^2Q_\nu^4}, \quad \theta = \frac{\pi}{4}. \tag{49}$$

This length is proportional to Q_ν^{-4}, in contrast to the Q_ν^{-2} dependence applicable for any incidence angle away from the Brewster angle. However, its wavelength dependence of order $O(\lambda^2)$ remains the same for all angles less than the critical angle. In the case of weak disorder ($Q_\nu \ll 1$), this means that the localization length can be made arbitrarily large at the Brewster anomaly angle relative to that realizable at other incidence angles.

Then, using Eq. (43) in Eq. (23), we may deduce that the characteristic wavelength λ_2 is identical to that obtained for s polarization Eq. (40). Similarly, λ_1, obtained using Eq. (48), is given by

$$\lambda_1 = \frac{\pi Q_\nu}{\cos\theta}\sqrt{\frac{2N}{3}}\sqrt{\cos^2 2\theta + \frac{Q_\nu^2}{\cos^2\theta}h_1(\theta)}. \quad (50)$$

The significance of the threshold wavelengths λ_1 and λ_2 is the same as for *s* polarization. Waves with $\lambda < \lambda_1$ are localized while the wavelength range $\lambda_1 < \lambda < \lambda_2$ corresponds to the near ballistic regime. Similarly, the ballistic length b has the same form as the localization length [Eq. (49)]

$$b = \frac{45\lambda^2}{16\pi^2 Q_\nu^4}, \quad \theta = \frac{\pi}{4}. \quad (51)$$

Thus, the transition from localization to the near ballistic regime takes place without any change in the scale. The wavelength range $\lambda > \lambda_2$ is the far ballistic region in which the ballistic length b_f is given by

$$\frac{1}{b_f} = \frac{k^2 Q_\nu^2 \cos^2 2\theta}{6\cos^2\theta}\left(1 + \frac{Q_d^2}{3}\right) + \frac{Nk^2 Q_\nu^4}{18\cos^2\theta}\left(\frac{3}{2} - \cos^2\theta\right)^2. \quad (52)$$

We emphasize that the results obtained in this section are applicable only to homogeneous stacks composed of normal material or metamaterial layers.

C. Long-wave asymptotics for mixed stacks

1. Mixed stacks: s polarization

Substituting the asymptotic forms in Eqs. (30)–(32) into Eqs. (16) and (17), we derive an expression for the reciprocal transmission length

$$\frac{1}{l_N} = \frac{k^2 Q_\nu^2}{3\cos^2\theta}\left(\frac{1}{2} - \frac{1 - f(N\alpha_s)}{3 + \zeta\cos^4\theta}\right), \quad (53)$$

where

$$\alpha_s = \frac{k^2 Q_\nu^2}{3\cos^2\theta}(3 + \zeta\cos^4\theta), \quad (54)$$

the function f is as defined in Eq. (18), and

$$\zeta = \frac{2Q_d^2}{Q_\nu^2}. \quad (55)$$

Equation (53) describes the transition from localization to ballistic propagation at long wavelengths and, in the limit as $N \to \infty$, we obtain the following expression for the localization length:

$$l = \frac{3\lambda^2\cos^2\theta}{2\pi^2 Q_\nu^2}\frac{3 + \zeta\cos^4\theta}{1 + \zeta\cos^4\theta}. \quad (56)$$

The ballistic length formally corresponds to the opposite extreme, i.e., as $N \to 0$,

$$b = \frac{3\lambda^2\cos^2\theta}{2\pi^2 Q_\nu^2} \quad (57)$$

and coincides with the result for a H-stack in *s* polarization.

The characteristic wavelengths λ_1 and λ_2 take the form

$$\lambda_1 = \frac{\pi Q_\nu}{\cos\theta}\sqrt{\frac{2N}{3}}\sqrt{\frac{1 + \zeta\cos^4\theta}{3 + \zeta\cos^4\theta}}, \quad (58)$$

$$\lambda_2 = \frac{\pi Q_\nu}{\cos\theta}\sqrt{\frac{4N}{3}}\sqrt{3 + \zeta\cos^4\theta}. \quad (59)$$

Again, for the range $\lambda \le \lambda_1(N)$, waves are localized while ballistic propagation occurs for very long wavelengths $\lambda \ge \lambda_2(N)$. The transition wavelengths $\lambda_{1,2}$ are of the same order and the intermediate region $\lambda_1(N) < \lambda < \lambda_2(N)$ corresponds to the crossover between localization and ballistic propagation.

2. Mixed stacks: p polarization

While we have derived a general expression for the transmission length that is applicable at arbitrary angles of incidence for a M-stack in *p* polarization, its form is quite complex and so it is presented only in the Appendix. In what follows, we look at a number of particular cases.

For incidence at angles away from the Brewster angle, the transmission length, according to Eq. (A1), is given by

$$\frac{1}{l_N} = \frac{k^2 Q_\nu^2 \cos^2 2\theta}{3\cos^2\theta}\left(\frac{1}{2} - \frac{1 - f(N\alpha_p)}{2 + \cos^2 2\theta + \zeta\cos^4\theta}\right), \quad (60)$$

where

$$\alpha_p = \frac{k^2 Q_\nu^2}{3\cos^2\theta}(2 + \cos^2 2\theta + \zeta\cos^4\theta). \quad (61)$$

The localization length may be deduced from Eq. (60) by taking the limit as $N \to \infty$, i.e.,

$$l = \frac{3\lambda^2\cos^2\theta}{2\pi^2 Q_\nu^2\cos^2 2\theta}\frac{2 + \cos^2 2\theta + \zeta\cos^4\theta}{\cos^2 2\theta + \zeta\cos^4\theta}. \quad (62)$$

Correspondingly, the ballistic length may be obtained by calculating the limit as $N \to 0$ in Eq. (60)

$$b = \frac{3\lambda^2\cos^2\theta}{2\pi^2 Q_\nu^2\cos^2 2\theta}. \quad (63)$$

The transmission length for the Brewster anomaly angle can be deduced by substituting $\theta = \pi/4$ in Eq. (A1)

$$\frac{1}{l_N} = \frac{4k^2 Q_\nu^4}{45}\left[1 + \frac{121 Q_\nu^2}{60}\frac{\left(1 - \frac{5\zeta}{44}\right)^2}{1 + \frac{\zeta}{8}}f(N\alpha_p)\right]. \quad (64)$$

Here, the second term in parentheses is always smaller than the first and therefore, at the Brewster angle, the transmission length as a function of the wavelength exhibits the same dependence, i.e.,

$$l_N = l = b = \frac{45\lambda^2}{16\pi^2 Q_\nu^4} \quad (65)$$

and is independent of the length of the stack. The transmission length in the localized regime for *p* polarization behaves as $O(Q_\nu^{-4})$ and exceeds the localization length far from the Brewster angle. Note that the localization length Eq. (65) for the M-stack at $\theta = \pi/4$ is the same as for the homogeneous stack Eq. (49).

The transition between the localized and ballistic regimes is again described by two characteristic wavelengths λ_1 and λ_2

$$\lambda_1 = \frac{\pi Q_\nu \cos 2\theta}{\cos\theta}\sqrt{\frac{4N}{3}}\sqrt{\frac{\cos^2 2\theta + \zeta\cos^4\theta}{2+\cos^2 2\theta+\zeta\cos^4\theta}}, \quad (66)$$

$$\lambda_2 = \frac{\pi Q_\nu}{\cos\theta}\sqrt{\frac{4N}{3}}\sqrt{4+2\cos^2 2\theta+\zeta\cos^4\theta}. \quad (67)$$

The expression for λ_1 [Eq. (66)] is obtained under the assumption that the angle of incidence is sufficiently far from the Brewster angle. At the Brewster angle, λ_1 and λ_2 are given by

$$\lambda_1 = \frac{4\pi Q_\nu^2}{3}\sqrt{\frac{N}{5}}, \quad (68)$$

$$\lambda_2 = 4\pi Q_\nu\sqrt{\frac{2N}{3}}\sqrt{1+\frac{\zeta}{16}}. \quad (69)$$

Note that $\lambda_2 \gg \lambda_1$. This means that at the Brewster angle, waves such that $\lambda \le \lambda_1(N)$ are localized while the ballistic region $\lambda_1(N) \le \lambda$ becomes divided into two subregions. The near ballistic subregion is bounded by the two characteristic lengths, i.e., $\lambda_1(N) \le \lambda \le \lambda_2(N)$, and the far ballistic region corresponds to very long waves $\lambda_2(N) \le \lambda$. As we explained previously, the localization length and the ballistic lengths in each of the two ballistic subregions are described by the same expression [Eq. (65)].

IV. RESULTS OF NUMERICAL SIMULATIONS

We now present results of our comprehensive numerical study of the properties of the transmission length as a function of wavelength and angle of incidence. Results are presented for direct simulations based on exact recurrence relations in Eqs. (3) and (4) and are compared with those obtained from the analytic forms in Eqs. (15)–(17), (21), and (22), and their short- and long-wavelength asymptotic forms derived in Sec. III.

A. Homogeneous stacks

1. Subcritical angle of incidence

We consider transmission through a H-stack characterized by the parameters: $Q_\nu = 0.1$ and $Q_d = 0.2$ at the incidence angle $\theta = 45°$, which is less than the critical angle $\theta_c = \sin^{-1}(0.9) \approx 64.16°$ and coincides with the Brewster anomaly angle for a layer with a mean refractive index of $\nu = 1$.

We begin with *s* polarization, and consider a stack of length $N = 10^4$, using $N_r = 10^4$ realizations for ensemble averaging. For the given parameters, the characteristic wavelengths are $\lambda_1 \approx 36$ and $\lambda_2 \approx 8.9 \times 10^4$. Plotted in Fig. 2 is the transmission length as a function of wavelength. Figure 2(a) corresponds to relatively short wavelengths $\lambda \le 10^2$ and represents mainly the localized part of the spectrum where $N \ge l_N \approx l$. Figure 2(b) corresponds to longer waves and mostly displays the ballistic part of the spectrum where $l_N \ge N$. In both panels, the red solid lines represent $l_N(\lambda)$, obtained by exact numerical simulation, and the blue dashed lines display the analytical form in Eq. (21). The excellent agreement between these two curves for all wavelengths (in both panels) is evident.

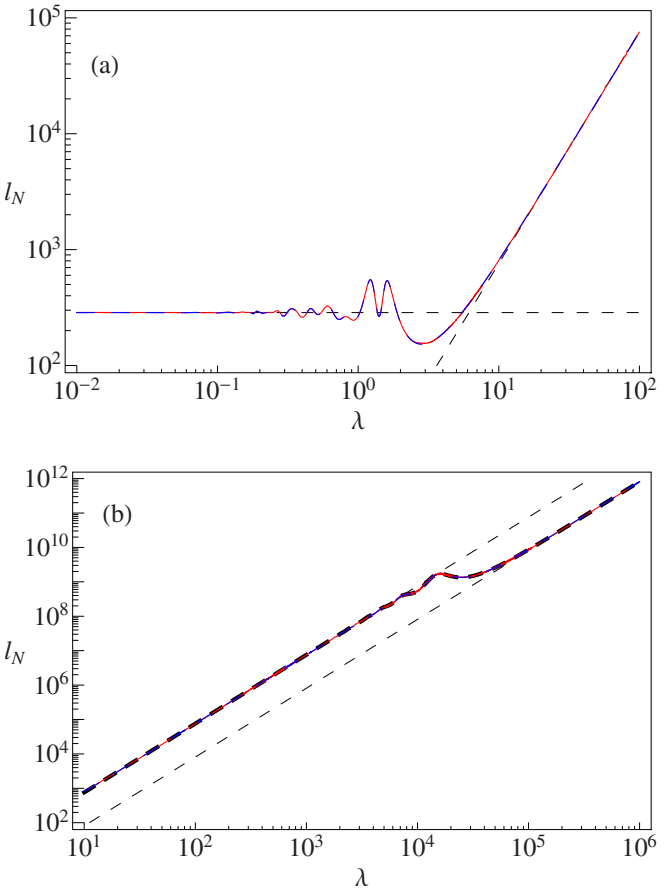

FIG. 2. (Color online) Transmission length l_N versus wavelength λ for $Q_\nu = 0.1$, $Q_d = 0.2$, and $\theta = 45°$ for *s*-polarized waves; panels (a) localized part of the spectrum and (b) ballistic part of the spectrum. Red solid curve: numerical simulation; blue dashed curve analytic form in Eq. (21).

The curves displayed in Fig. 2(a) explicitly confirm the coincidence of the long-wave asymptotes of the transmission length in both the localized ($\lambda < 36$, $l_N = l$) and near ballistic ($36 < \lambda$, $l_N = b$) regions. The slanted, dashed line corresponds to the asymptotic forms in Eqs. (35) and (36) while the horizontal dashed line corresponds to the short-wave asymptote Eq. (25). The corresponding curves of Fig. 2(b) display the transmission length in the ballistic regime. The near ballistic region, where $l_N = b$, occurs for $36 \le \lambda \le 8.9 \times 10^4$, while the transition to the far ballistic region, where $l_N = b_f$, occurs for $\lambda \approx 8.9 \times 10^4$. The upper and lower dashed lines, respectively, display the near and far ballistic lengths of Eqs. (36) and (38). We observe that the results for *s* polarization are entirely consistent with those reported previously for the case of normal incidence.[24]

Figure 3 presents the corresponding results for the case of *p*-polarized waves. Here, we consider a much longer stack of $N = 10^6$ layers, the characteristic wavelengths of which are

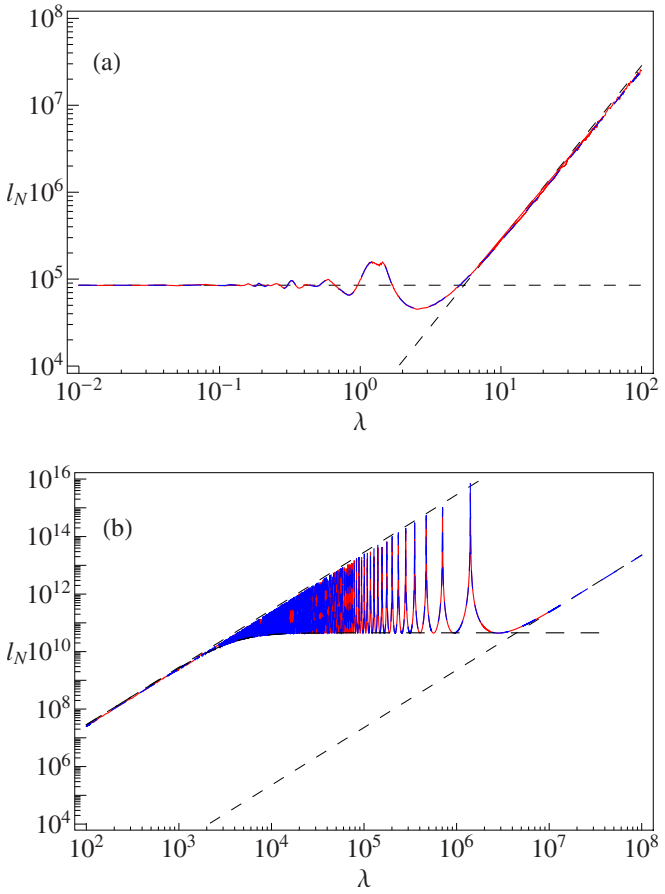

FIG. 3. (Color online) Transmission length l_N versus λ for $Q_\nu=0.1$, $Q_d=0.2$ for *p*-polarized waves at the Brewster anomaly angle $\theta=45°$. Panel (a) localized part of the spectrum; panel (b) the transition from localization to ballistic propagation. Red solid curve: numerical simulation; blue dashed curve: analytic form in Eq. (21).

$\lambda_1 \approx 19$ and $\lambda_2 \approx 8.9\times 10^6$. Figure 3(a) displays the transmission-length spectrum for comparatively short wavelengths $\lambda \le 10^2$ and corresponds mainly to the localized part of the spectrum where $N \ge l_N \approx l$. The results of Fig. 3(b) correspond to longer waves $\lambda \ge 10^2$ and display the ballistic part of the spectrum $\lambda \ge \lambda_1$ where $l_N \ge N$. In both panels, the red solid and the blue dashed lines, respectively, display $l_N(\lambda)$ obtained by exact numerical calculation and the analytic form in Eq. (21), and we see that their agreement is excellent.

The results of Fig. 3(a) show that the long-wave asymptote of the transmission length in both the localized region $\lambda < 19$ (where $l_N=l$), and the near ballistic region $19<\lambda<10^2$ (where $l_N=b$) coincide exactly. The slanted dashed line corresponds to the asymptotic form in Eq. (49) while the horizontal dashed line represents the short-wave asymptote Eq. (24). We observe that the short- and long-wave limits for the localization length at the Brewster angle are proportional to Q_ν^{-4} and hence are two orders larger than in the case of *s* polarization. These numerical results confirm the analytical results presented earlier in Sec. III B 2.

Figure 3(b) characterizes the ballistic regime which comprises a near ballistic region $(19 \le \lambda \le 8.9\times 10^6)$ in which $l_N=b$ and a far ballistic region where $l_N=b_f$ with the transition between the two occurring at $\lambda \approx 8.9\times 10^6$. The upper and lower dashed lines, respectively, display the asymptotes for the near [Eq. (51)] and far [Eq. (52)] ballistic lengths. The ballistic length, over the entire ballistic region, including the transition from the near to far ballistic regime, is very well described by Eq. (47). The oscillatory nature of this transition is due to Fabry-Perot resonances between the first and the last interfaces of the stack and is much more pronounced than for the case of *s* polarization. We observe that the envelope of the transmission-length curve is confined from below by Eq. (47) in which the sine term is replaced by unity. This is the long dashed black curve of Fig. 3(b). While this highly oscillatory region also occurs for *s*-polarized waves, it is not apparent in Fig. 2 since the chosen stack length ($N=10^4$) was not sufficiently long to exhibit the feature.

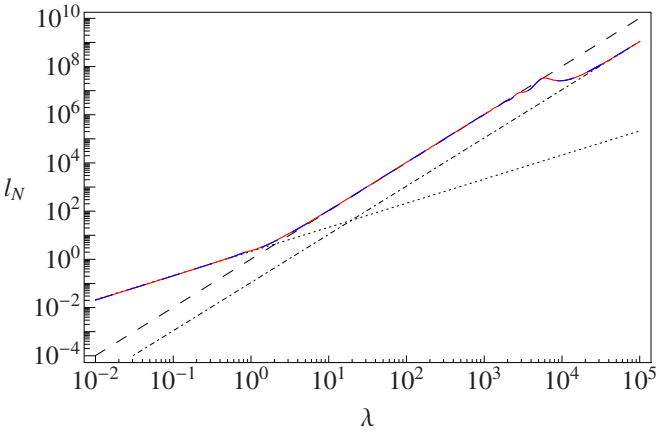

FIG. 4. (Color online) Transmission length l_N of the homogeneous stack with $N=10^4$, $Q_\nu=0.1$, and $Q_d=0.2$ versus wavelength λ for *s*-polarized waves at the supercritical incidence angle $\theta=75°$. Red solid curve: numerical simulation; blue dashed curve analytic form in Eq. (21).

In the samples with only refractive-index disorder (i.e., $Q_d=0$), the localization length displays strong oscillations at intermediate wavelengths $0.3<\lambda<2$ for both polarizations. Equation (22) is also in an excellent agreement with the numerical calculations. We also note that the thickness disorder smears out these oscillations with only few oscillations remaining for $Q_d=0.2$ (see Figs. 2 and 3).

2. Supercritical angle of incidence

When the angle of incidence exceeds the critical angle, i.e., $\theta > \theta_c = \sin^{-1}(1-Q_\nu)$, the exponential wave decay can be attributed not only to Anderson localization but also to attenuation inside the individual layers. In Fig. 4, we plot the transmission-length spectrum for a *s*-polarized wave in which the parameters of the problem are the same as for Fig. 2, apart from the angle of incidence which is $\theta=75°$. In this case, the characteristic wavelengths are $\lambda_1 \approx 99$ and $\lambda_2 \approx 3.2\times 10^4$. Since, as noted previously in Sec. III A, Eq. (21) can serve as a good interpolation formula for the transmission length in the short- and long-wave regions, we have plotted the results of the exact numerical simulation (red solid curve) together with those predicted by Eq. (21) (blue

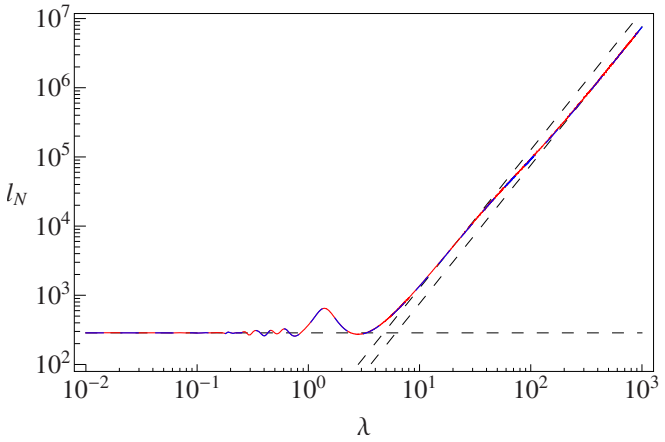

FIG. 5. (Color online) Transmission length versus λ for a M-stack in *s*-polarized light with $Q_\nu=0.1$, $Q_d=0.2$, and $N=10^4$ for $\theta=45°$. Red solid curve: numerical simulations; blue dashed curve: analytic form in Eq. (15).

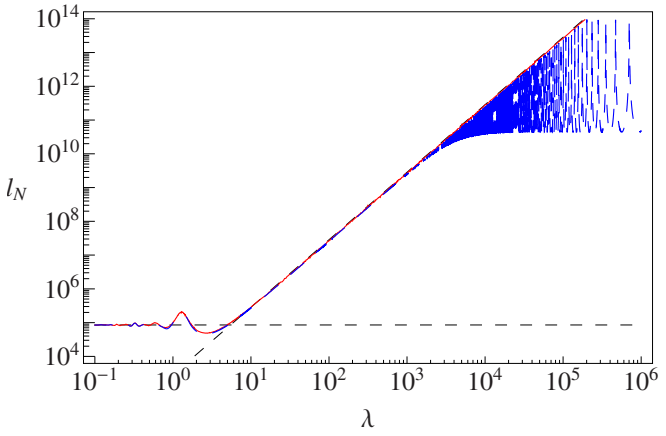

FIG. 6. (Color online) Transmission length versus λ for a M-stack in *p*-polarized light with $Q_\nu=0.1$, $Q_d=0.2$, and $N=10^6$, at the Brewster angle $\theta=45°$ red solid line. The blue dashed line shows results for *s* polarization and a H-stack, replotted for comparison.

dashed curve) to demonstrate the quality of the agreement.

In Fig. 4, the dotted line displays the short-wavelength asymptotic Eq. (29), the black dashed, slanted line displays the localization length Eq. (35), and the dashed dotted line shows the far ballistic asymptotic given by Eq. (38). At short wavelengths, $\lambda \leq 2$, the form of the transmission-length spectrum is determined mainly by attenuation or "tunneling" effects. The transmission length is proportional to the wavelength and is well described asymptotically by Eq. (29), the dotted black slanted line in Fig. 4. For longer waves, the form of the transmission length is the same as is observed below the critical angle and is described well by Eq. (34).

Anderson localization is realized only in the intermediate wavelength region, $2 \leq \lambda \leq 99$, with $l_N \approx l$ with the localization length given by Eq. (35) and shown in the black dashed slanted line of Fig. 4. For *p* polarization, the spectral behavior of the transmission length is qualitatively equivalent to that for *s* polarization and so we do not present this here. There is excellent agreement between the exact numerical calculation, the theoretical result of Eq. (22), and the short- [Eq. (24)] and long- [Eq. (48)] wave asymptotic forms.

B. Mixed stacks

1. Subcritical angle of incidence

We first consider the case of *s*-polarized wave propagation through a mixed (i.e., alternating layers of normal and metamaterials) stack of length $N=10^4$. The parameters are the same as those adopted in Sec. IV A 1, i.e., $Q_\nu=0.1$, $Q_d=0.2$, $N_r=10^4$, and the incidence angle is $\theta=45°$, which is less than the critical angle $\theta_c=\sin^{-1}(0.9)=64.16°$ and coincides with the Brewster angle for the single layer with mean refractive index $\nu=\pm 1$. For these parameters, the characteristic wavelengths given by Eqs. (58) and (59) are $\lambda_1 \approx 28$ and $\lambda_2 \approx 115$ correspondingly.

In Fig. 5, the red solid line and the blue dashed line, respectively, display results from the numerical simulation and the analytic form (based on the WSA) for the transmission length as a function of wavelength with these two coinciding to high accuracy.

The form of the transmission-length spectrum is similar to that observed for the case of normal incidence.[24] The short-wavelength asymptotic form in Eq. (24), shown as the horizontal dashed line in Fig. 5, is the same as for a H-stack. For $\lambda \leq \lambda_1 = 28$, all waves are localized with the localization length Eq. (56) shown by the upper dashed, slanted straight line. The transition from localization to ballistic propagation occurs in the wavelength range $\lambda_1 < \lambda < \lambda_2$ and is well described by Eq. (53). Ballistic propagation occurs for $\lambda \geq \lambda_2 = 115$ and is characterized by the ballistic length Eq. (57) which differs from the M-stack localization length Eq. (53), in contrast to the case of H-stacks.

Figure 6 displays the transmission-length spectrum for a M-stack of length $N=10^6$ in *p*-polarized light with all other parameters identical to that for the *s*-polarization simulations. In this case, the characteristic wavelengths are $\lambda_1 \approx 19$ [from Eq. (66)] and $\lambda_2 \approx 1200\pi$ [from Eq. (67)].

The results of the numerical simulation and the WSA analytical forms in Eqs. (15) and (16) coincide and are displayed by a single red solid line. Localization occurs for $\lambda \leq \lambda_1 \approx 19$ while the transition from localization to ballistic propagation occurs at $\lambda \sim \lambda_1$. In contrast to the case of *s* polarization, the transition is not accompanied by a change in scale and is given by the same wavelength dependence Eq. (65). The same asymptotic Eq. (65) also holds for wavelengths $\lambda > \lambda_2 \approx 1200\pi$, which defines the transition from the near to the ballistic regime. As a consequence of the disorder $Q_\nu = 0.1$, the short-wave localization length Eq. (24) (horizontal dashed line) is two orders of magnitude larger than that for *s*-polarized light (cf. Fig. 5).

2. Supercritical angle of incidence

We now consider a case in which the angle of incidence $\theta=75°$ exceeds the critical angle $\theta_c=\sin^{-1}(1-Q_\nu)=64.16°$ [Eq. (11)]. In Fig. 7 we present the transmission-length spectrum for *s*-polarized light and display results from the exact

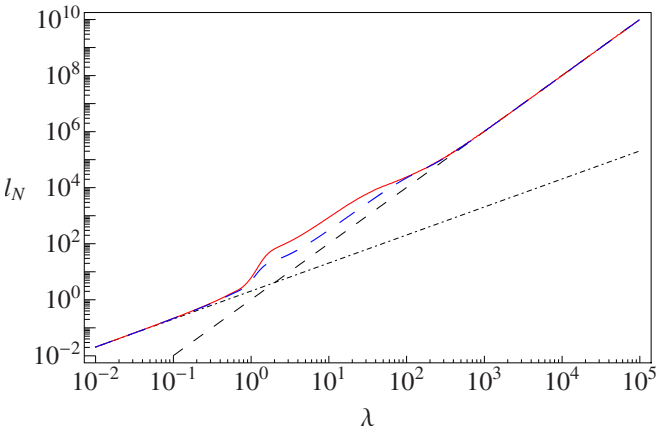

FIG. 7. (Color online) Transmission length versus λ for a M-stack in *s*-polarized light with $Q_\nu=0.1$, $Q_d=0.2$, and $N=10^4$, and for the supercritical incidence angle $\theta=75°$. Red solid curve: numerical simulations; blue dashed curve: analytic form in Eq. (15).

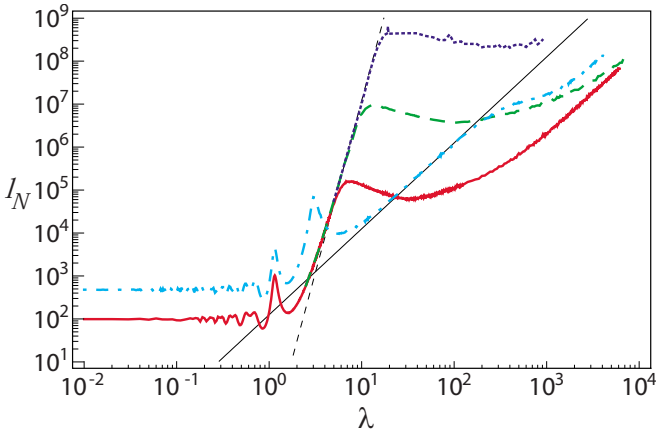

FIG. 8. (Color online) Transmission length l_N versus λ for a M-stack with $Q_\nu=0.25$, $Q_d=0$, and $\theta=30°$ for *p*-polarized light (cyan dashed dotted curve, $N=10^6$) and *s*-polarized light (red solid curve, $N=10^5$; green dashed curve, $N=10^7$; and blue dotted curve, $N=8\times10^8$).

numerical calculation (red solid line) and the analytic form (long dashed blue curve). The expectation that Eq. (15) would serve as a good interpolation formula for the transmission length in the short- and long-wave regions, as anticipated in Sec. III A, is borne out by the results of Fig. 7. The short-wave (dashed dotted line) asymptotic form in Eq. (29) and the long-wave (black dashed line) asymptotic form in Eq. (57), respectively, coincide with the numerical results for $\lambda\leq1$ and $200\leq\lambda$. In the intermediate region $1\leq\lambda\leq200$, however, the theoretical description underestimates the actual transmission length since the WSA is no longer valid for the chosen, supercritical angle of incidence. For *p* polarization, the results are qualitatively the same but with the discrepancy at the intermediate wavelengths even more pronounced.

C. Mixed stacks with refractive-index disorder

In our earlier paper,[23] we demonstrated that at normal incidence a disordered mixed stack, with only refractive-index disorder, could substantially suppress Anderson localization. Indeed, the suppression is so strong that even the usual quadratic dependence on wavelength [i.e., $O(\lambda^2)$] of the localization length at long wavelengths was shown to change to $O(\lambda^6)$. In contrast, the introduction of the thickness disorder in combination with the refractive-index disorder induces strong localization at long wavelengths with the localization length returning to its expected quadratic dependence on wavelength.[24] In this section, we consider the effects of polarization on long-wavelength localization in M-stacks.

Figure 8 displays transmission-length spectra for a mixed stack with only refractive-index disorder for an angle of incidence of $\theta=30°$. Four curves are displayed: for *p*-polarized light and a stack of length $N=10^6$ (dashed doted cyan curve) and for *s*-polarized light and three stacks of lengths $N=10^5$ (solid red curve), $N=10^7$ (dashed green curve), and $N=8\times10^8$ (blue curve). There is a striking difference between the two polarizations: in the case of *p*-polarized light, there is strong localization at long wavelengths ($\lambda\leq10^2$) with the localization length showing $O(\lambda^2)$ dependence; in contrast, the localization length for *s*-polarized light is much larger and shows the $O(\lambda^6)$ dependence as occurs for normal incidence. Note that for *s* polarization, the localization regions in Fig. 8 are bounded from above by the wavelength limits $\lambda\leq5$, 9, and 12 for stacks of length $N=10^5$, 10^7, and 8×10^8, respectively.

This asymmetry between the polarizations suggests that the suppression of localization is due not only to the suppression of the phase accumulation but also to the vector nature of the electromagnetic wave. Because of the symmetry of Maxwell's equations between the electric and magnetic fields, it is to be expected that for a model in which there is disorder in the magnetic permeability (with $\varepsilon=\pm1$) the situation will be inverted with localization for *p*-polarized waves being suppressed and with *s* polarization showing strong localization.

In concluding this section, we emphasize that the delicate phenomenon of the suppression of localization occurs only for refractive-index disorder and that the introduction of any thickness disorder leads to the strong localization (see Sec. IV B 1 and Ref. 24).

V. TRANSMISSION LENGTH AS A FUNCTION OF THE INCIDENCE ANGLE

A. Homogeneous stacks

We next consider the angular dependence of the transmission length of a homogeneous stack for a given wavelength. As in earlier simulations, we work with the parameters $Q_\nu=0.1$, $Q_d=0.2$, and $N=10^6$. Figure 9 displays the transmission length as a function of the angle of incidence θ for both *s* and *p* polarizations. In each panel (upper: $\lambda=0.1$, lower: $\lambda=10$), the solid red curve displays the results of the numerical simulation while the blue dashed line corresponds to the WSA analytic form in Eq. (22) with the top and bottom sets being for *p* and *s* polarizations, respectively.

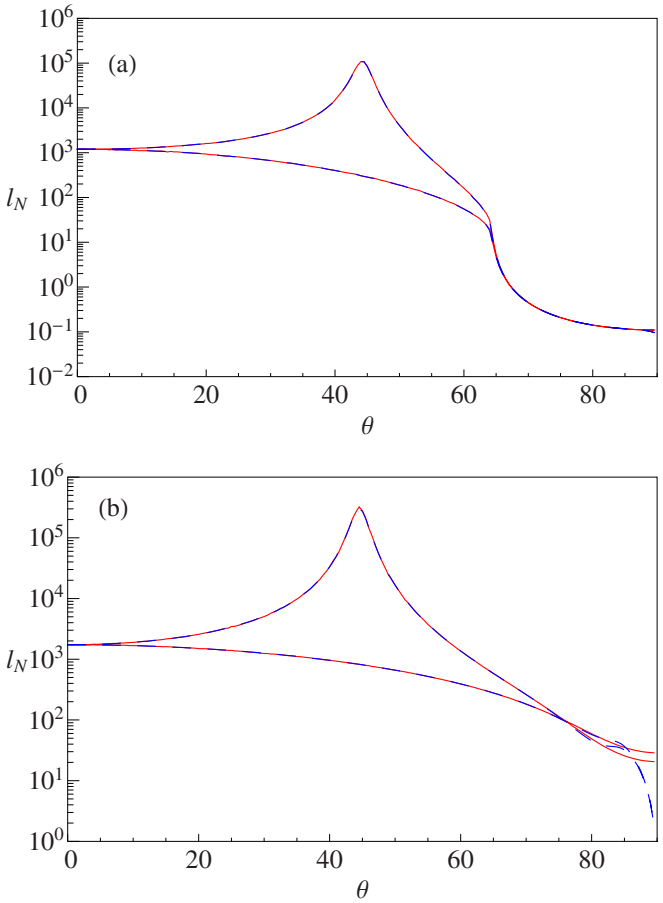

FIG. 9. (Color online) Transmission length l_N versus incidence angle θ for a homogeneous stack with Q_v=0.1, Q_d=0.2 for (a) λ =0.1 (upper panel), (b) λ=10 (lower panel). Red solid curve: numerical simulations; blue dashed curve analytic form in Eq. (22). The top set of curves in each of the panels are for p polarization while the bottom set of curves are for s polarization.

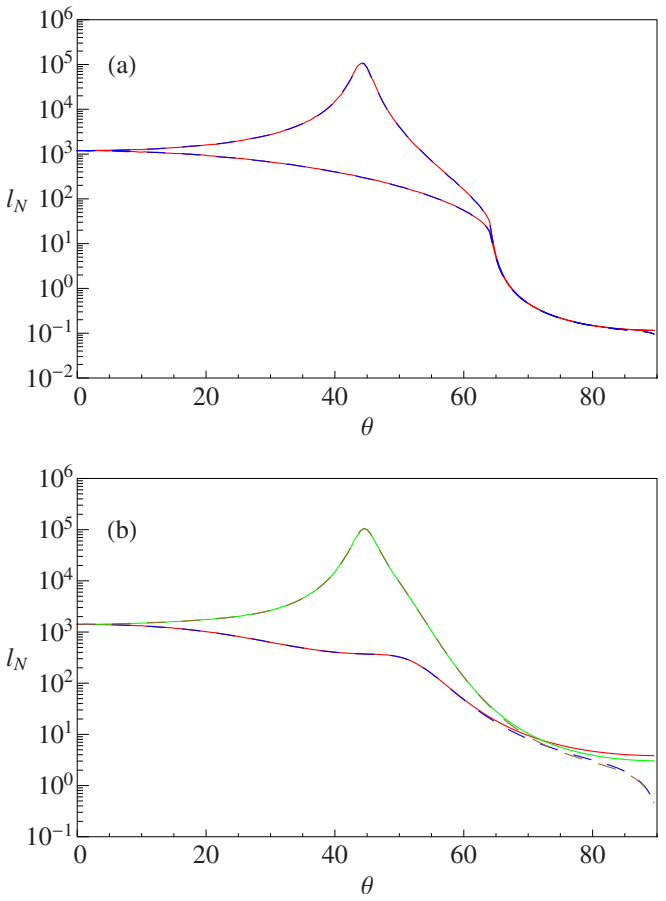

FIG. 10. (Color online) Transmission length l_N versus incidence angle θ for a mixed stack with Q_v=0.1, Q_d=0.2, for (a) λ=0.1 (upper panel) and (b) λ=1 (lower panel). The top and bottom curves are, respectively, for p and s polarizations.

For the short wavelength λ=0.1 [Fig. 9(a)], the analytic form agrees perfectly with the simulations. While for s polarization, the transmission length decreases monotonically with the angle of incidence, the transmission length for p polarization displays a pronounced maximum at the Brewster anomaly angle (at $\theta \approx 46°$ for these parameters). In the supercritical regime, $\theta > \theta_c \approx 64°$, attenuation is the dominant mechanism for localization and hence the behavior of the two polarizations coincide.

For long wavelengths, as in Fig. 9(b), we see that for extreme angles of incidence (e.g., for $\theta > 80°$ for the wavelength λ=10), the theoretical prediction departs markedly from the simulation results. Similar departures for intermediate wavelengths (e.g., for λ=1) also exist for angles of incidence $\theta > 85°$.

We have also calculated the localization length for the very long wavelength of λ=40 as a function of the angle of incidence (for the same parameters as for Fig. 9), for which the expansion Eq. (48) is applicable. There is excellent agreement between the exact numerical calculation and the asymptotic form in Eq. (48) for angles of up to 80°. [Since this plot is very similar to Fig. 9(b), it is not included in the paper.]

B. Mixed stacks

We now consider the angular dependence of the transmission length for mixed stacks and, in Fig. 10, we plot l_N as a function of the angle θ for a stack of length $N=10^6$ at the two wavelengths λ=0.1 [Fig. 10(a)] and λ=1 [Fig. 10(b)]. In either case, the calculated transmission length does not exceed the stack length and so, for subcritical angles, our calculations display the true localization length. For the shorter wavelength λ=0.1, the form of the transmission length for both polarizations is similar to that observed for homogeneous stacks [cf. Fig. 9(a)], and we also note that the analytical form in Eq. (16) agrees perfectly with the results from the numerical simulations.

Figure 10(b) displays results for an intermediate wavelength λ=1 with the lower solid red and blue dashed curves, respectively, displaying the results of numerical simulations and analytical predictions in Eq. (16) for s polarization, (bottom curves) while the upper solid green and brown dashed curves display simulations and analytical predictions in Eq. (16) for p polarization. The agreement between simulations and the theoretical form is again excellent for angles of incidence less then the critical angle, $\theta < \theta_c$, while for angles greater then the critical angle, the discrepancies that are evident are again explicable by the breaking down of the WSA at extreme angles of incidence.

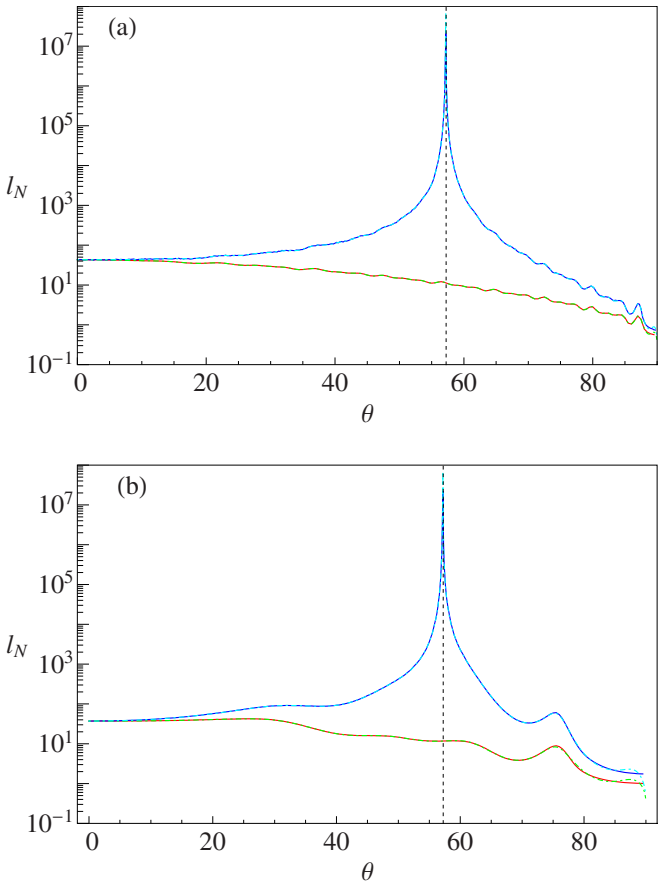

FIG. 11. (Color online) Delocalization at the Brewster angle θ_B: (a) at a short wavelength $\lambda=0.1$ and (b) an intermediate wavelength $\lambda=0.5$. Top and bottom curves are, respectively, for p and the s polarizations.

C. Alternating homogeneous stacks

In this section, we present an example of true delocalization arising from the vector nature of the electromagnetic field. This was first pointed out by Sipe *et al.*,[10] in which an analysis applicable at long wavelengths was presented. More recently, the analysis has been extended to short wavelengths.[11] The condition for the Brewster anomaly can be satisfied for a homogeneous stack (i.e., with all layers being either normal materials or all being metamaterials) with only thickness disorder and with alternating refractive indices (i.e., with refractive indices ν_A and ν_B, respectively, for odd and even numbered layers).

We proceed in a similar manner to that of Ref. 10 and consider a stack in vacuum with $\nu_A=1$ and $\nu_B=1.5$ and with layers whose random thicknesses are uniformly distributed in the interval $d\in[0.8,1.2]$ (i.e., $Q_d=0.2$). We note that in the case of p polarization, the applicability of the weak scattering approximation is heightened in the vicinity of the Brewster angle since each layer is almost transparent.

In Figs. 11(a) and 11(b), we, respectively, plot the transmission length as a function of the angle of incidence at a short wavelength $\lambda=0.1$, and also at an intermediate wavelength $\lambda=0.5$. The lower and upper curves are, respectively, for s and p polarizations, and we see, somewhat surprisingly, that the numerical simulations and the analytic forms obtained within a WSA framework are essentially identical for both polarizations for arbitrary incidence angles, apart from the discrepancies evident for extreme angles $\theta>87°$ at $\lambda=0.5$. The surprising element is that the theoretical framework based on the WSA appears to work over a much wider range of angles and polarizations than that suggested by strict validity of the WSA. In the figure, the theoretical description for s polarization (green curve) overlays the results of the numerical calculation (red curve). The same is true for p polarization with the theoretical prediction (black dotted line) overlaying results from the numerical calculation (cyan solid curve).

In these calculations, the stack length was $N=10^4$ and so waves are delocalized for incidence angles $55°\leq\theta\leq59°$ around the Brewster angle $\theta_B=\arctan(1.5)\approx56.19°$ where the transmission length $l_N\geq N$. The localization properties for the corresponding homogeneous stack composed of metamaterial layers with $\nu_B=-1.5$ is the same as that shown in Fig. 11 for normal layers with $\nu_B=1.5$. The WSA-based theory also appears to work over a reasonably broad range of wavelengths, although for the intermediate wavelengths $10\leq\lambda\leq50$ there are some differences between simulations and the theoretical prediction.

VI. CONCLUSIONS

We have investigated the effect of polarization on the Anderson localization in one-dimensional disordered stacks composed entirely of either right- or left-handed layers, as well as mixed stacks with alternating sequence of normal and metamaterial layers.

Our analysis has generalized the results obtained earlier[24] for the case of normal incidence to the case of an arbitrary angle of incidence with a particular attention paid to the localization at the Brewster angle. Based on this approach, we have carried out a comprehensive study of the localization length as a function of both the angle of incidence and the polarization of the incident wave for various types of disorder.

In the case of general disorder, where both refractive index and thickness of the layers are random, we have derived the long- and short-wave asymptotics for the localization length for a wide range of incidence angles, including the Brewster angle. At the Brewster angle, we have shown that the localization length continues to exhibit a quadratic dependence on wavelength (as in the case of the normal incidence), but that the coefficient of proportionality becomes parametrically larger, being proportional to Q^{-4}, rather than Q^{-2} ($Q\ll1$), as for the case of the normal incidence.

Our theoretical study not only characterizes the localization and ballistic propagation but also describes perfectly the crossover between these two regimes. We have also shown that the transition from localization to ballistic propagation in the vicinity of the Brewster angle in a mixed stack is given by a single scale Eq. (65). In the case of thickness disorder, we have shown that, at the Brewster angle, Anderson localization is suppressed completely.

ACKNOWLEDGMENTS

This work was supported by the Australian Research Council through its Discovery Grants program. We also acknowledge the provision of computing facilities through the National Computational Infrastructure in Australia.

APPENDIX: TRANSMISSION LENGTH FOR *p* POLARIZATION AND MIXED STACK

In this appendix, we provide an asymptotic form for the transmission length in the case of *p* polarization for a mixed stack. The reciprocal transmission length Eq. (15) takes the form

$$\frac{1}{l_N} = \frac{k^2 Q_\nu^2}{6\cos^2\theta}\cos^2 2\theta\left(1+\frac{Q_d^2}{3}\right) + \frac{k^2 Q_\nu^4}{40\cos^2\theta}(2-3\cos 2\theta)^2\left(1+\frac{Q_d^2}{3}\right) + \frac{k^2 Q_\nu^6}{4}(2-3\cos 2\theta)\left(1+\frac{Q_d^2}{3}\right)\tan^2\theta$$
$$+ \frac{k^2 Q_\nu^8}{48}(43-55\cos 2\theta)\tan^2\theta - \frac{\frac{2k^2 Q_\nu^4\cos^2 2\theta}{3\cos^2\theta} + f_1 + f_2 + f_3 + f_4 + f_5}{2Q_\nu^2(2+\cos^2 2\theta) + 4Q_d^2\cos^4\theta} + \frac{\frac{4k^2 Q_\nu^4\cos^2 2\theta}{3\cos^2\theta} + g_1 + g_2 + g_3 + g_4 + g_5}{4Q_\nu^2(2+\cos^2 2\theta) + 8Q_d^2\cos^4\theta} f(N\alpha_p), \tag{A1}$$

where

$$f_1 = \frac{k^2 Q_\nu^4 Q_d^2}{24\cos^2\theta}\left(\frac{61}{8} + \frac{25}{6}\cos 2\theta + \frac{19}{3}\cos 4\theta - \frac{5}{6}\cos 6\theta + \frac{\cos 8\theta}{24}\right), \tag{A2}$$

$$f_2 = \frac{k^2 Q_\nu^6}{12\cos^2\theta}\left(\frac{1927}{120} - \frac{121}{5}\cos 2\theta + \frac{403}{30}\cos 4\theta - \frac{49}{15}\cos 6\theta + \frac{\cos 8\theta}{24}\right), \tag{A3}$$

$$f_3 = \frac{k^2 Q_\nu^6 Q_d^2}{32\cos^2\theta}\left(\frac{7013}{270} - \frac{1763}{45}\cos 2\theta + \frac{3772}{135}\cos 4\theta - \frac{1391}{135}\cos 6\theta + \frac{163}{270}\cos 8\theta\right), \tag{A4}$$

$$f_4 = \frac{k^2 Q_\nu^8}{32\cos^2\theta}\left(\frac{633}{4} - \frac{19058}{75}\cos 2\theta + \frac{9521}{75}\cos 4\theta - \frac{818}{25}\cos 6\theta + \frac{593}{300}\cos 8\theta\right), \tag{A5}$$

$$f_5 = \frac{k^2 Q_\nu^4 Q_d^4}{864\cos^2\theta}(3+10\cos 2\theta - \cos 4\theta)^2 \tag{A6}$$

and

$$g_1 = \frac{2k^2 Q_\nu^6}{45\cos^2\theta}(46-77\cos 2\theta + 41\cos 4\theta - 11\cos 6\theta), \tag{A7}$$

$$g_2 = \frac{k^2 Q_\nu^4 Q_d^2}{18\cos^2\theta}(10+5\cos 2\theta + 10\cos 4\theta - \cos 6\theta), \tag{A8}$$

$$g_3 = \frac{k^2 Q_\nu^8}{270\cos^2\theta}\left(1963 - \frac{16534}{5}\cos 2\theta + \frac{8968}{5}\cos 4\theta - \frac{2362}{5}\cos 6\theta + \frac{121}{5}\cos 8\theta\right), \tag{A9}$$

$$g_4 = \frac{k^2 Q_\nu^6 Q_d^2}{60\cos^2\theta}\left(\frac{247}{3} - 139\cos 2\theta + \frac{928}{9}\cos 4\theta - \frac{103}{3}\cos 6\theta + \frac{11}{9}\cos 8\theta\right), \tag{A10}$$

$$g_5 = \frac{k^2 Q_\nu^4 Q_d^4}{432\cos^2\theta}(3+10\cos 2\theta - \cos 4\theta)^2. \tag{A11}$$

The expansion Eq. (A1) is valid for any angle of incidence for mixed stacks at long wavelengths. The factor f is given by Eq. (18) in this expression and characterizes the transition from localization to ballistic propagation.

For the sake of completeness, we also provide in this appendix the expression for the cubic coefficient a in the expansion Eq. (42).

$$a = (1+Q_d^2)\left[\frac{iQ_\nu^2}{36\cos\theta}(3+18\cos 2\theta-\cos 4\theta)+\frac{iQ_\nu^4}{480\cos^3\theta}(146-87\cos 2\theta+158\cos 4\theta-41\cos 6\theta)\right.$$
$$\left.+\frac{iQ_\nu^6}{336\cos^3\theta}(365-604\cos 2\theta+331\cos 4\theta-86\cos 6\theta)\right]+\frac{iQ_\nu^8\tan^2\theta}{48\cos\theta}(175-264\cos 2\theta+107\cos 4\theta). \quad \text{(A12)}$$

All expansions in Eqs. (30)–(32) and (41)–(43) and in the appendix can be readily obtained by using symbolic manipulation package such as MATHEMATICA.

[1] P. W. Anderson, Phys. Rev. **109**, 1492 (1958).
[2] I. M. Lifshitz, S. A. Gredeskul, and L. A. Pastur, *Introduction to the Theory of Disordered Systems* (Wiley, New York, 1989).
[3] S. John, Phys. Rev. Lett. **53**, 2169 (1984).
[4] P. Sheng, *Introduction to Wave Scattering, Localization, and Mesoscopic Phenomena* (Academic, San Diego, 2007).
[5] A. Lagendijk, B. van Tiggelen, and D. S. Wiersma, Phys. Today **62**(8), 24 (2009).
[6] V. D. Freilikher, M. Pustilnik, and I. Yurkevich, Phys. Rev. Lett. **73**, 810 (1994).
[7] J. C. J. Paasschens, T. Sh. Misirpashaev, and C. W. J. Beenakker, Phys. Rev. B **54**, 11887 (1996).
[8] A. A. Asatryan, N. A. Nicorovici, L. C. Botten, C. M. de Sterke, P. A. Robinson, and R. C. McPhedran, Phys. Rev. B **57**, 13535 (1998).
[9] P. Sheng, *Scattering and Localization of Classical Waves in Random Media* (World Scientific, Singapore, 1991), p. 589.
[10] J. E. Sipe, P. Sheng, B. S. White, and M. H. Cohen, Phys. Rev. Lett. **60**, 108 (1988).
[11] K. Yu. Bliokh and V. D. Freilikher, Phys. Rev. B **70**, 245121 (2004).
[12] V. D. Freilikher and S. A. Gredeskul, Prog. Opt. **30**, 137 (1992).
[13] N. Mott and Twose, Adv. Phys. **10**, 107 (1961).
[14] H. Furstenberg, Trans. Am. Math. Soc. **108**, 377 (1963).
[15] V. Baluni and J. Willemsen, Phys. Rev. A **31**, 3358 (1985).
[16] C. M. de Sterke and R. C. McPhedran, Phys. Rev. B **47**, 7780 (1993).
[17] G. A. Luna-Acosta, F. M. Izrailev, N. M. Makarov, U. Kuhl, and H. J. Stockmann, Phys. Rev. B **80**, 115112 (2009).
[18] F. M. Izrailev, N. M. Makarov, and E. J. Torres-Herrera, Physica B **405**, 3022 (2010).
[19] V. G. Veselago, Sov. Phys. Usp. **10**, 509 (1968).
[20] J. B. Pendry, Phys. Rev. Lett. **85**, 3966 (2000).
[21] K. Yu. Bliokh and Yu. P. Bliokh, Phys. Usp. **47**, 393 (2004) [Usp. Fiz. Nauk **174**, 439 (2004)].
[22] P. Marcos and C. M. Soukoulis, *Wave Propagation from Electrons to Photonic Crystals and Left-Handed Materials* (Princeton University Press, Princeton, 2008).
[23] A. A. Asatryan, L. C. Botten, M. A. Byrne, V. D. Freilikher, S. A. Gredeskul, I. V. Shadrivov, R. C. McPhedran, and Y. S. Kivshar, Phys. Rev. Lett. **99**, 193902 (2007).
[24] A. A. Asatryan, S. A. Gredeskul, L. C. Botten, M. A. Byrne, V. D. Freilikher, I. V. Shadrivov, R. C. McPhedran, and Y. S. Kivshar, Phys. Rev. B **81**, 075124 (2010).
[25] V. Malyshkin, A. R. McGurn, J. M. Elson, and P. Tran, Waves Random Media **8**, 203 (1998).
[26] X. Du, D. Zhang, X. Zhang, B. Feng, and D. Zhang, Phys. Rev. B **56**, 28 (1997).